Journal of Cluster Science (2023) 34:1535–1546
https://doi.org/10.1007/s10876-022-02326-2

ORIGINAL PAPER

$(NH_4)_2[Co(H_2O)_6]_2V_{10}O_{28}\cdot 4H_2O$ Vs. $(NH_4)_2[Ni(H_2O)_6]_2V_{10}O_{28}\cdot 4H_2O$: Structural, Spectral and Thermal Analyses and Evaluation of Their Antibacterial Activities

Ayat-Allah Mamdouh[1] · Ahmed B. M. Ibrahim[1] · Nour El-Houda A. Reyad[2] · Tarek R. Elsayed[3] · Isabel Cordeiro Santos[4] · António Paulo[4] · Refaat M. Mahfouz[1]

Received: 7 November 2021 / Accepted: 10 July 2022 / Published online: 28 July 2022

Abstract
This paper presents the synthesis of two cluster compounds {$(NH_4)_2[Co(H_2O)_6]_2V_{10}O_{28}\cdot 4H_2O$ (**C1**) and $(NH_4)_2[Ni(H_2O)_6]_2V_{10}O_{28}\cdot 4H_2O$ (**C2**)} which were obtained as single crystals suitable for XRD analysis that revealed their crystallization in the monoclinic (C2/c) and triclinic (P-1) space groups, respectively. Additionally, **C1** and **C2** were characterized using CHN analysis and FT-IR spectroscopy and their thermal decomposition mechanisms were investigated. The antibacterial activities of both compounds were determined against three human pathogenic bacterial strains {*Bacillus cereus* ATCC 33,018, *Escherichia coli* O157:H7 and *Pseudomonas aeruginosa* ATCC 9027} and one phytopathogenic bacterial strain {*Ralstonia solanacearum*}, while drug standards {chloramphenicol and streptomycin} were used as control. The inhibitory activity and the minimum inhibitory concentration (MIC) values of the tested compounds clearly indicated higher antibacterial activities of the nickel compound against *B. cereus* ATCC 33,018, *E. coli* O157 and *R. solanacearum* with MIC values of 3.150, 3.150 and 6.300 mg/ml, respectively. On the other hand, $(NH_4)_2[Co(H_2O)_6]_2V_{10}O_{28}\cdot 4H_2O$ exhibited higher antibacterial activity against *P. aeruginosa* ATCC 9027 (MIC value of 6.300 mg/ml) in comparison to the nickel analog. In general, the measured activities are lower than that obtained for the standards except for the higher activity given by **C2** in comparison to streptomycin against the *R. solanacearum* strain.

Keywords Decavanadate clusters · d-element complexes · XRD · Bacterial pathogens · Antimicrobial agents

Introduction

Polyoxometalates (POMs) are 3D negatively charged species of an accumulation of oxide clusters with a variety of transition metals, e.g. vanadium, molybdenum and tungsten [1]. These compounds are diversely applicable in electrochemistry [2], catalysis [3, 4], magnetochemistry [5], photochemistry [6] and medicine [7]. Pure inorganic POMs can show synergistic or direct antibacterial activity: Generally most of the inorganic POMs exhibit insignificant antibacterial activity at pharmacologically acceptable concentrations and the activities are enhanced in synergy with conventional antibiotics [8]. Nevertheless, twenty pure inorganic POMs were tested as direct antibacterial agents against six strains of *Streptococcus pneumoniae* and the polyoxovanadates (POVs) displayed high antibacterial activities whereas the other POMs that contained molybdenum and tungsten gave insignificant activities [9].

The polyoxovanadates (POVs), as a subclass of POMs, are divided into families of V(III), V(IV), V(V), V(IV)/V(III) and V(V)/V(IV) species and the family of V(V) clusters includes $[V_2O_7]^{-4}$ [10], $[V_3O_9]^{-3}$ [11], $[V_4O_{12}]^{-4}$ [12], $[V_5O_{14}]^{-3}$ [13], $[V_{10}O_{28}]^{-6}$ [14], $[V_{12}O_{32}]^{-4}$ [15], $[V_{13}O_{34}]^{-3}$ [16], $[V_{15}O_{42}]^{-9}$ [17] and $[V_{16}O_{42}]^{-4}$ [18] species. The superb behavior of POVs is attributed to their structural

✉ Ahmed B. M. Ibrahim
aibrahim@aun.edu.eg

1 Department of Chemistry, Faculty of Science, Assiut University, Assiut 71516, Egypt

2 Plant Pathology Department, Faculty of Agriculture, Cairo University, Giza, Egypt

3 Microbiology Department, Faculty of Agriculture, Cairo University, Giza, Egypt

4 Centro de Ciências e Tecnologias Nucleares, Instituto Superior Técnico, Universidade de Lisboa, Estrada Nacional 10 (km 1397), 2695-066 Bobadela LRS, Portugal

diversity that permits numerous utilizations in medicine, biological processes, topology, geochemistry and energy-related applications [19–21].

The roles of vanadium-based compounds in biology are varied spanning from amending the activity of phosphatases [22], ATPase [23] and myosin [24] to inhibiting phosphofructokinase, hexokinase, adenylate kinase and tyrosine kinase [25–27]. This is in addition to the involvement of vanadium compounds as inorganic cofactors in alternative nitrogenases and haloperoxidases, and their relevance in the development of anticancer agents and insulin-mimetic agents [28–31]. The antibacterial activities of decavanadates, condensed {VO6} octahedra sharing vertices and edges [14], were reported against e.g. *E. coli, K. pneumonia, S. marcescens, S. plymuthica* and *P. aeruginosa* [32], and their activities were mostly attributed to the production of high amounts of reactive oxygen species [33].

On the other hand, cobalt and nickel are elements of superlative significance involved in biology. Cobalt is regarded as an essential element [34] and the applicability of several cobalt complexes is presumably due to their aqueous stability, availability and ease of synthesis [35] in addition to their in vivo insulin-like [36], anti-fungal and anti-oxidant [37] properties. Nickel is biologically involved in several enzymes, e.g. Ni–Fe hydrogenase, urease, acetyl-CoA decarbonylase/synthase, CO dehydrogenase, various superoxide dismutases, methyl coenzyme M reductase, methylenediurease, some glyoxylases and aci-reductonedioxygenase [38–40]. Various cobalt and nickel complexes have displayed activities against Gram-positive and Gram-negative bacteria, e.g. a cobalt complex of the anti-ulcer drug "famotidine" possessed antibacterial activities against *M. lysodeikticus* and *E. coli* higher than that of the free drug [41–46] and two complexes of nickel with amidodithiophosphonates showed good anti-proliferative activities against *S. aureus* and *S. haemolyticus* strains [47]. The combination of Co(II) or Ni(II) with V(V) systems is quite rare in biology and biomedical applications. Nevertheless, a recent study reported enhanced anti-bacterial activities for cobalt-vanadium oxides {$Co_3(VO_4)_2$ and CoV_2O_6} in comparison to V_2O_5 [48] and another study confirmed that a synergistic reaction between Ni(II) and V(V) system resulted in impairing the microbial growth and survival [49].

This paper presents the synthesis and single-crystal structures of two cluster compounds, $(NH_4)_2[Co(H_2O)_6]_2V_{10}O_{28}\cdot 4H_2O$ (**C1**) and $(NH_4)_2[Ni(H_2O)_6]_2V_{10}O_{28}\cdot 4H_2O$ (**C2**), which in addition were studied by FT-IR spectroscopy and by thermal analysis (a group of techniques in which a property of the sample is monitored against time or temperature, and the temperature of the sample is programmed in a specific atmosphere). Taking into consideration the importance of introducing inorganic antibacterial agents in alternative to organic bactericides that usually suffer from a short life span and cause environmental pollution, we here assessed the antibacterial activities of **C1** and **C2** against three human pathogenic bacterial strains (*B. cereus* ATCC 33,018, *E. coli* O157:H7 and *P. aeruginosa* ATCC 9027) and one phytopathogenic bacterial strain (*R. solanacearum*), in comparison to reference drugs.

Materials and Methods

Physical Measurements

The starting chemicals, ammonium metavanadate, ammonium tartarate, cobalt chloride hexahydrate and nickel chloride hexahydrate, are analytical grade Alfa Aesar and Merck products and were used as received. For the synthesized compounds, the hydrogen and nitrogen contents were measured on Elementar Analysensysteme GmbH—vario EL III Element Analyzer and the infrared spectral data as KBr pellets were determined on a Nicolet iS10 spectrophotometer. The cluster compounds were studied by thermogravimetric (TG) analyses up to 500 °C in the air under the heating rate of 10 degrees/min on a Shimadzu DTG 60-H thermal analyzer. Selected crystals of compounds **C1** and **C2** were mounted on loops with protective oil and the X-ray data were collected on a Bruker APEX II diffractometer using graphite monochromated MoKα radiation (λ = 0.71073 Å) at 150(2) K operating in a φ and ω scans mode. The X-ray generator was operated at 50 kV and 30 mA and the data were monitored by the APEX [50] program. All data were corrected for Lorentzian, polarization and absorption effects using SAINT and SADABS [51] programs. SHELXT 2014 [52] and SHELXL 2014 [52] were respectively used for structure solution and for full matrix least-squares refinement on F^2. These two programs are included in the WINGX-v2014.1 [53] program package. Non-hydrogen atoms were refined with anisotropic thermal parameters. The H-atoms of the water molecules and NH_4 ions were located from the electron density map and allowed to refine freely. Molecular graphics, polyhedral representation of anion and packing diagrams, were drawn using Mercury 2020 [54]. Symmetry transformations {(-x + 1/2,-y + 3/2,-z + 1) and (-x + 1,-y,-z + 2)} were used to generate the equivalent atoms of the $(V_{10}O_{28})^{6-}$ anion in **C1** and **C2**, respectively. In (**C1**), a water molecule (O1S) was disordered over two positions with 0.5 occupancy factor.

Synthesis of the Clusters

For the synthesis of $(NH_4)_2[Co(H_2O)_6]_2V_{10}O_{28}\cdot 4H_2O$ (**C1**) and $(NH_4)_2[Ni(H_2O)_6]_2V_{10}O_{28}\cdot 4H_2O$ (**C2**), a mixture of ammonium metavanadate NH_4VO_3 (5.85 g, 50 mmol),

ammonium tartrate (4.60 g, 25 mmol) and water (200 ml) was boiled under vigorous stirring until complete dissolution of the reagents. To this solution, the appropriate hexahydrated metal chloride (25 mmol; 5.94–5.95 g) was added with stirring. After stirring for 1 h at room temperature, any solids were removed by filtration. The products were recovered as single crystals by filtration from the reaction solutions after keeping them undisturbed at room temperature for a week. The crystals were washed with water and ethanol and dried in the air.

C1: Yield (478 mg, 6.8% based on vanadium). Anal. Calcd. (Found) % for $Co_2V_{10}H_{40}N_2O_{44}$ (MW = 1399.58 g/mol) = H, 2.88 (3.01)% and N, 2.00 (2.13)%. FT-IR (KBr disk, cm^{-1}): 3373 (br), 3191 (s), 1619 (s), 1420 (s), 961 (s), 822 (m), 741(m), 579 and 519 (m).

C2: Yield (1.43 g, 20.4% based on vanadium). Anal. Calcd. (Found) % for $Ni_2V_{10}H_{40}N_2O_{44}$ (MW = 1399.10 g/mol) = H, 2.88 (3.05)% and N, 2.00 (2.14)%. FT-IR (KBr disk, cm^{-1}): 3396 (br), 3171 (s), 1623 (s), 1418 (s), 947 (s), 823 (m), 740 (m), 579 (m) and 519 (m).

Antibacterial Activity

The antibacterial activity of the two cluster compounds was determined against three human pathogenic bacterial strains (*B. cereus* ATCC 33,018, *E. coli* O157:H7 and *P. aeruginosa* ATCC 9027) obtained from the American type culture collection and one locally isolated phytopathogenic bacterial strain (*R. solanacearum*). The inhibitory activity and the antibacterial agent lowest concentration that allows visible growth inhibition of the bacterial strains (minimum inhibitory concentrations, MIC) were determined by applying the broth dilution method [55]. In this method, bacterial strains are tested for their ability to generate visible growth in broth containing dilutions of the antimicrobial agent as follows: Twenty-four hours broth culture of each bacterial pathogen was performed by inoculation of a single colony into an Erlenmeyer flask containing 100 ml of trypticase soy broth and by incubation at 37 °C for *B. cereus*, *E. coli* and *P. aeruginosa* and at 30 °C for *R. solanacearum*. In the solidified Mueller–Hinton agar medium (Beef infusion: 300.0 g, Casein acid hydrolysate: 17.5 g, Starch: 1.5 g, Agar: 17.0 g, and 1000 ml of water) that permits good growth of most nonfastidious pathogens and is also low in antagonists, four wells of 8 mm diameter each were made using a sterilized cork borer and one hundred microliters from each culture were spread on the surface of the solidified agar medium. Five concentrations of each antibacterial agent were prepared in water and fifty microliters of each solution were added to each well, while chloramphenicol (for *B. cereus*, *E. coli* and *P. aeruginosa*) and streptomycin (for *R. solanacearum*) were added to the control plates. The antibacterial agents diffused into the agar medium and allowed for bacterial inhibition. The tests were performed in triplicate and the inhibition zone diameters (expressed in mm) were assessed after 48 h.

Results and Discussion

Chemistry

The polyoxovanadate based compounds, $(NH_4)_2[Co(H_2O)_6]_2V_{10}O_{28}{\bullet}4H_2O$ (**C1**) and $(NH_4)_2[Ni(H_2O)_6]_2V_{10}O_{28}{\bullet}4H_2O$ (**C2**), were isolated from reaction mixtures containing the desired hydrated metal chloride {$CoCl_2.6H_2O$/$NiCl_2.6H_2O$}, ammonium metavanadate and ammonium tartrate. All reagents were mixed in water at boiling temperature, before cooling the solutions to room temperature and allowing them to stand undisturbed for seven days. After this time, the clusters **C1** and **C2** were isolated as single crystals which exhibited air and light stability for months. In the reactions, every ten ions of VO_3^- polymerized to produce the cluster anion $V_{10}O_{28}^{6-}$ that attracted ammonium counter ions and hydrated cobalt and nickel ions for the assembly of the products. Indeed, the ammonium tartrate was added seeking the isolation of inorganic–organic clusters similar to others described in the literature [56]. However, the CHN analyses of the compounds indicated the absence of carbon revealing the absence of the tartrate anion in the products.

For the determination of the crystal structure of the products, single crystals of **C1** (0.140 × 0.100 × 0.040 mm) and **C2** (0.300 × 0.250 × 0.150 mm) were analyzed by XRD diffraction studies (Table 1). The compound **C1** crystallized in monoclinic C2/c space group and the compound **C2** crystallized in triclinic P-1 space group.

The asymmetric units contain one (NH_4), two H_2O, half ($V_{10}O_{28}$) and one [$Co(H_2O)_6$] for **C1** or one [$Ni(H_2O)_6$] for **C2**. Figure 1 shows the asymmetric units of the solved structures extended by inversion centre {(**C1**) (-x + 1/2,-y + 3/2,-z + 1) and (**C2**)(-x + 1,-y,-z + 2)} to obtain the cluster anion $V_{10}O_{28}^{6-}$. Figure 2 displays the projection of the crystal packing, viewed along the [001] direction for compounds **C1** and **C2**, showing the arrangement of $V_{10}O_{28}^{6-}$ anionic units isolated from each other by the cations {NH_4 and $Co(H_2O)_6$ or $Ni(H_2O)_6$} and H_2O molecules.

Selected bond distances for the structures of compounds **C1** and **C2** are listed in Table 2, while Table 3 includes selected angles for each structure. In compounds **C1** and **C2**, the Co(II) and Ni(II) cations are six-coordinate with water oxygen atoms (O15-O20 in compound **C1** and O16-O21 in compound **C2**). The Co(II) ion in **C1** lies in the center of a slightly distorted octahedron with trans O—Co—O angles in the range 174.59(8)-176.59(8)° and Co—O distances in the range 2.077(2) Å—2.103(2) Å (average = 2.0875 Å).

Table 1 Crystal and structure refinement data for compounds **C1** and **C2**

Cluster compound	**C1**	**C2**
Empirical formula	$Co_2H_{40}N_2O_{44}V_{10}$	$Ni_2H_{40}N_2O_{44}V_{10}$
Formula weight	1399.58	1399.10
Crystal system	Monoclinic	triclinic
Space group	C 2/c	P -1
a (Å)	17.0630(3)	8.7569(2)
b (Å)	13.9596(2)	10.8882(2)
c (Å)	16.9967(3)	11.0741(3)
α (°)	90	65.2877(8)
β (°)	115.0090(10)	73.4048(9)
γ (°)	90	71.3735(9)
Volume (Å^3)	3668.91(11)	894.64(4)
Z	8	1
Calculated density (g/cm^3)	2.534	2.597
μ (mm^{-1})	3.436	3.648
F(000)	2760	692
θ range for data collection (°)	2.918 to 26.368	2.749 to 26.372
Reflections collected	29,882	8704
Unique refl. collected (R_{int})	3743(0.0502)	3631(0.0380)
Completeness to theta	99.8%	99.8%
Absorption correction	Semi-empirical from equivalents	Semi-empirical from equivalents
Max. and min. transmission	0.875 and 0.645	0.611 and 0.407
GOF on F^2	1.053	1.062
R_1 [I > 2σ(I)]	0.0216	0.0251
wR2 (all data)	0.0614	0.0661
Largest diff. peak, hole/e Å^{-3}	0.584 and −0.602	0.416 and −0.457
CCDC number	2,095,582	2,095,581

The corresponding angles and bond distances in compound **C2** are in the ranges 172.84(9)-176.55(9)° and 2.040(3) Å—2.074(2) Å (average = 2.052 Å). In the decavanadate anions, the shortest V—V contacts are 3.04 and 3.052 Å in compounds **C1** and **C2**, respectively. All V atoms are six-coordinate with the V—O bond distances varying according to the respective bond order. In the cluster anion $\{V_{10}O_{28}^{6-}\}$, four of the oxygen atoms are terminal (denoted as O1, O6, O9 and O11 in compound **C1** and as O5, O7, O11 and O14 in compound **C2**), seven are μ_2-bridged (denoted as O2, O3, O4, O5, O8, O10 and O14 in compound **C1** and as O1, O2, O3, O4, O8, O12 and O15 in compound **C2**), two are μ_3-bridged (denoted as O7 and O12 in compound **C1** and as O9 and O10 in compound **C2**) and one is μ_6-bridged (denoted as O13 in compound **C1** and as O6 in compound **C2**). In compound **C1**, the terminal V = O bond distances are in the range 1.604(2) Å (V3—O9) to 1.628(2) Å (V2—O6)Å, the μ_2(O)—V distances in the range 1.673(2) Å (O14—V5) to 2.097(1) Å (O14^i—V3), the μ_3(O)—V distances in the range 1.931(2) Å (O7—V5) to 2.029(1) Å (O12^i —V2) and the μ_6(O)—V distances in the range 2.116(1) Å (O13—V5) to 2.308(1) Å (O13^i—V1). In its turn, the nickel compound **C2** exhibits the following ranges of distances for the different types of V—O bonds: terminal V = O, 1.599(2) Å (V1—O5) to 1.610(2) Å (V2—O7); μ_2(O)—V, 1.683(2) Å (O15^i—V4) to 2.065(2) Å (O15—V5); μ_3(O)—V, 1.904(2) Å (O10^i—V4) to 2.003(2) Å (O10—V2); μ_6(O)—V, 2.109(2) Å (O6^i—V4) to 2.347(2) Å (O6—V1).

In both compounds, the oxygen atoms from the decavanadate anion act as acceptors in three-dimensional hydrogen bond networks with ammonium ions and H_2O molecules as the donors (Table 4).

The FT-IR spectra of compound **C1** and compound **C2** are presented in Fig. 3. The sharp bands appearing in the spectra of the Co(II) and Ni(II) cluster compounds at 961 and 947 cm^{-1}, respectively, are due to stretching vibrations υ(V = O_t) of the terminal oxygen-vanadium bonds (O_t = terminal oxygen) [57]. The asymmetric stretching vibrations of the bridging oxygen O_b – vanadium bonds υ_{as}(V—O_b) display frequencies of 822 and 741 cm^{-1} for compound **C1** and 823 and 740 cm^{-1} for compound **C2** [58–60]. The symmetric stretching vibrations of the same bonds υ_s(V—O_b) originate medium intensity bands at lower wavenumbers of 519 and 579 cm^{-1} for **C1** and **C2** [61]. The broad bands in the spectra of compound **C1** and compound **C2** appearing at frequencies around 3373 and 3396 cm^{-1} can be assigned to asymmetric and symmetric vibrations υ(O—H) of lattice water molecules [62, 63]. The sharp bands located at around 1619 and 1623 cm^{-1} in the spectra of compound **C1** and compound **C2**, respectively, are due to the δ(H—O—H) bending vibrational modes of these water molecules [64]. The peaks at 3191 and 1420 cm^{-1} in the spectrum of **C1** and at 3171 and 1418 cm^{-1} in the spectrum of **C2** correspond, respectively, to symmetric and asymmetric stretching vibrations of the N—H bonds from the tetrahedral ammonium cation [60, 64].

Thermogravimetric analysis (thermal gravimetric analysis or TGA) is a technique in thermal analysis in which a change in the mass of a material is observed due to increase in temperature. The TGA curves of compounds **C1** and **C2** are presented in Fig. 4. Both compounds, when heated up to 500 °C, decomposed to stable residual products corresponding to 75.495 and 75.407% of the original mass, respectively. In detail, compound **C1** decomposed in overlapped steps up to 264 °C (mass loss = 20.621%) in addition to a clear decomposition step up to the temperature of 373 °C (mass loss = 3.884%). Indeed, these weight losses are corresponding to the removal of sixteen solvated water molecules (Calcd. = 20.595%) and two ammonia (from the decomposition of the ammonium ions) and one extra water molecule (two protons from the ammonium ions and one oxygen atom from the decomposition of the decavanadate anion) (Calcd. = 3.721%). Therefore, the resulting

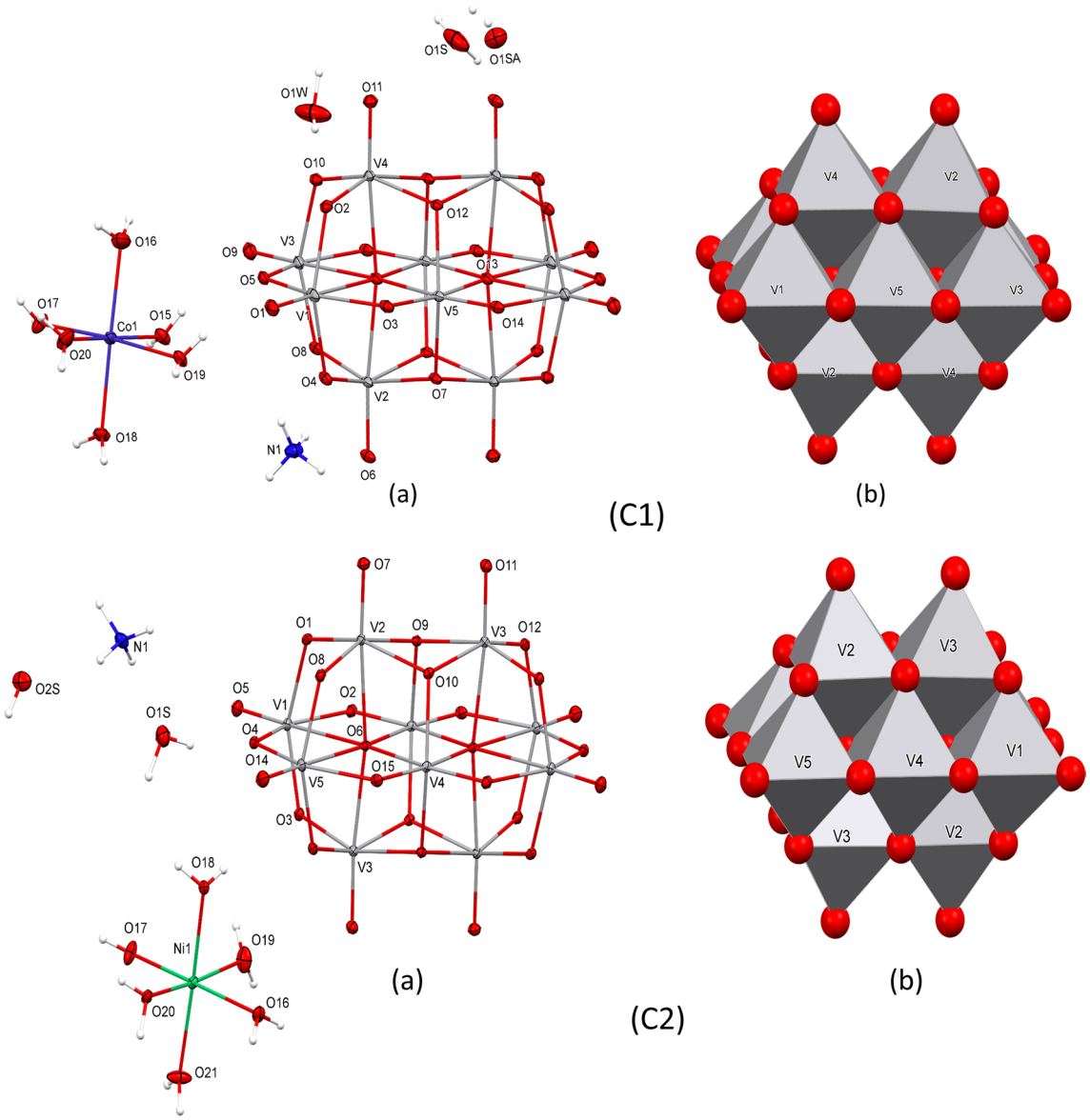

Fig. 1 **a** Molecular structures of **C1** (top) and **C2** (bottom) with atomic numbering of the asymmetric units and thermal ellipsoids drawn at 40%, and **b** polyhedral model of decavanadate anions ($V_{10}O_8^{6-}$) showing the central plane formed by six vanadium atoms and the other four positioned two above and two below this plane

residual product could be in the form of 2 $Co(VO_3)_2 + 3$ V_2O_5 (Calcd. = 75.684%). On the other hand, compound **C2** started decomposing at about 110 °C, which is a relatively higher temperature than the decomposition temperature observed for compound **C1**. However, it also decomposed in an overlapped decomposition step up to the temperature of 275 °C and a clear decomposition step in the range of 275–391 °C. The weight losses found for **C2** correspond to the removal of similar moieties as observed for the decomposition of compound **C1** {in fact, the observed mass loss of 20.966% (Calcd. = 20.601%) corresponds also to the removal of sixteen water molecules and that of 3.627% (Calcd. = 3.723%) corresponds to the removal of one water and two ammonia molecules}. Therefore, the residual product is proposed to be a composite mixture of $Ni(VO_3)_2$ and V_2O_5 (2:3) (Calcd. = 75.676%).

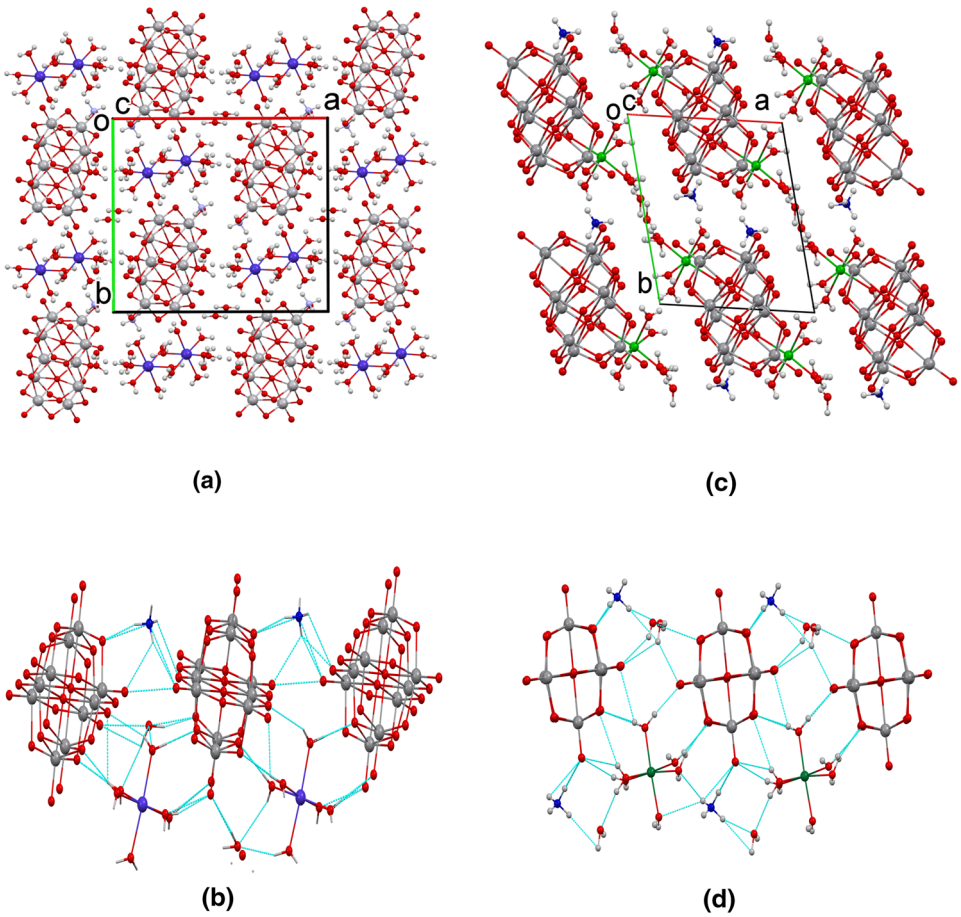

Fig. 2 Crystal packing viewed along *c* axis of **a** $(NH_4)_2[Co(H_2O)_6]_2V_{10}O_{28}$•$4H_2O$ (**C1**) and **c** $(NH_4)_2[Ni(H_2O)_6]_2V_{10}O_{28}$•$4H_2O$ (**C2**). **b** and **d** show structural interactions (blue dashed lines) of the decavanadate anions with cations and H_2O molecules in compounds **C1** and **C2**, respectively

Antibacterial Activity

The two cluster compounds, $(NH_4)_2[Co(H_2O)_6]_2V_{10}O_{28}·4H_2O$ (**C1**) and $(NH_4)_2[Ni(H_2O)_6]_2V_{10}O_{28}·4H_2O$ (**C2**), were tested for their antibacterial activities against four different human pathogens and phytopathogens representing Gram-positive and negative bacteria using the agar well diffusion assay method [55], with determination of inhibition zone diameters (Fig. 5) and minimum inhibitory concentrations (Table 5). Both compounds gave the same MIC value against *P. aeruginosa* ATCC 9027 and *R. solanacearum*, but **C2** displayed lower MIC values against *B. cereus* ATCC 33,018 and *E. coli* O157. Generally, the results revealed antibacterial activity of the two compounds against the four tested bacterial pathogens. However, the nickel compound (**C2**) displayed higher activities than the cobalt counterpart (**C1**) against *B. cereus* ATCC 33,018, *E. coli* O157 and *R. solanacearum* with MIC values of 3.150, 3.150 and 6.300 mg/ml, respectively. On the other hand, the cobalt compound displayed higher activity against *P. aeruginosa* ATCC 9027 even if both compounds showed the same MIC concentration of 6.300 mg/ml. In numbers, **C1** gave inhibition of 6 mm in the *B. cereus* culture only at a concentration of 12.60 mg/ml, while **C2** at concentrations of 3.150, 4.201, 6.300 and 12.60 mg/ml afforded inhibitions respectively of 3, 5, 6 and 9 mm. As a control, chloramphenicol (10 mg/ml) displayed an inhibitory activity of 10 mm. On the other hand, compounds **C1** and **C2** displayed antibacterial activities against *P. aeruginosa* ATCC 9027 and *R. solanacearum* only at concentrations equal to or higher than 6.300 mg/ml.

Table 2 Selected bond lengths (Å) in compounds **C1** and **C2**

$(NH_4)_2[Co(H_2O)_6]_2V_{10}O_{28}\bullet 4H_2O$ **C1**				$(NH_4)_2[Ni(H_2O)_6]_2V_{10}O_{28}\bullet 4H_2O$ **C2**			
Atoms	Length Å	Atoms Å	Length Å	Atoms	Length Å	Atoms	Length Å
Co1–O15	2.103(2)	V3–O5	1.792(1)	Ni1–O16	2.048(2)	V3–O9	1.999(2)
Co1–O16	2.089(3)	V3–O8	1.891(2)	Ni1–O17	2.040(3)	V3–O10	1.980(2)
Co1–O17	2.077(2)	V3–O9	1.604(2)	Ni1–O18	2.074(2)	V3–O11	1.606(2)
Co1–O18	2.089(2)	V3–O10	1.886(2)	Ni1–O19	2.046(2)	V3–O12	1.821(2)
Co1–O19	2.090(2)	V3–O13^{i}	2.307(1)	Ni1–O20	2.057(2)	V3–O3^{i}	1.839(2)
Co1–O20	2.077(2)	V3–O14^{i}	2.097(1)	Ni1–O21	2.047(2)	V3–O6^{i}	2.233(2)
V1–O1	1.611(1)	V4–O2	1.785(1)	V1–O1	1.902(2)	V4–O2	1.702(2)
V1–O2	1.917(2)	V4–O10	1.858(2)	V1–O2	2.025(2)	V4–O6	2.117(2)
V1–O3	2.001(2)	V4–O11	1.615(2)	V1–O3	1.873(2)	V4–O9	1.945(2)
V1–O4	1.922(2)	V4–O12	1.984(1)	V1–O4	1.846(2)	V4–O6^{i}	2.109(2)
V1–O5	1.915(1)	V4–O7^{i}	2.024(1)	V1–O5	1.599(2)	V4–O10^{i}	1.904(2)
V1–O13^{i}	2.308(1)	V4–O13^{i}	2.251(2)	V1–O6	2.347(2)	V4–O15^{i}	1.683(2)
V2–O4	1.772(1)	V5–O3	1.695(1)	V2–O1	1.831(2)	V5–O4	1.825(2)
V2–O6	1.628(2)	V5–O7	1.931(2)	V2–O6	2.231(2)	V5–O6	2.310(2)
V2–O7	1.997(2)	V5–O12	1.940(2)	V2–O7	1.610(2)	V5–O8	1.899(2)
V2–O8	1.843(1)	V5–O13	2.116(1)	V2–O8	1.813(2)	V5–O14	1.603(2)
V2–O12^{i}	2.029(1)	V5–O14	1.673(2)	V2–O9	2.002(2)	V5–O15	2.065(2)
V2–O13^{i}	2.256(2)	V5–O13^{i}	2.135(1)	V2–O10	2.003(2)	V5–O12^{i}	1.847(2)

Compound **C1** inhibited *P. aeruginosa* by 6 and 11 mm and **C2** by 4 and 8 mm at concentrations of 6.300 and 12.60 mg/ml, respectively. In this strain, chloramphenicol (10 mg/ml) displayed an inhibitory activity of 12 mm. For the same concentrations (6.300 and 12.60 mg/ml) and against the *R. solanacearum* strain, **C1** displayed inhibitory activities of 3 and 6 mm and **C2** afforded inhibitions of 8 and 12 mm, while the positive control (streptomycin (10 mg/ml)) showed an inhibitory activity of 8 mm that is given by lower concentration of 6.300 mg/ml of **C2** against *R. solanacearum*. Indeed, the least pronounced results were obtained against *E. coli* O157 for both compounds, as **C1** and **C2** showed activities not exceeding 1 mm for concentrations up to 12.60 mg/ml. In the same strain, chloramphenicol (10 mg/ml) displayed an inhibitory activity of 14 mm.

In fact, the activity difference between **C1** and **C2** is attributed to different activities of $[Co(H_2O)_6]^{2+}$ and $[Ni(H_2O)_6]^{2+}$ as these species interact differently with the active centers of the bacterium cell membrane. Additionally, this interaction could also be resulted from hydrogen bonding with the compounds due to the availability of donor and acceptor centers on the cluster compounds [65].

Conclusions

Two decavanadate based cluster compounds, $(NH_4)_2[Co(H_2O)_6]_2V_{10}O_{28}\cdot 4H_2O$ (**C1**) and $(NH_4)_2[Ni(H_2O)_6]_2V_{10}O_{28}\cdot 4H_2O$ (**C2**), were synthesized and their structures were determined by X-ray crystallography that revealed their stabilization through the formation of 3D networks based on extensive H-bonds. The compounds were further analyzed by FT-IR spectroscopy and thermal analysis that indicated overlapped steps of decomposition and decomposition to mixtures of vanadium (V) oxide and metal (II) vanadate $M(VO_3)_2$ (M = Co(II) or Ni(II)) at 500 °C. Both cluster compounds were tested as antibacterial agents against strains of different bacterial pathogens. The Ni cluster (**C2**) was more active against *B. cereus* ATCC 33,018, *E. coli* O157:H7 and *R. solanacearum*, while the *P. aeruginosa* ATCC 9027 strain was inhibited more intensively by the cobalt congener (**C1**). The antibacterial activities are lower than that of the standards, but **C2** (6.300 mg/ml) and streptomycin (10 mg/ml) against *R. solanacearum* strains afforded the same inhibition of 8 mm.

Table 3 Selected bond angles (°) in compounds **C1** and **C2**

$(NH_4)_2[Co(H_2O)_6]_2V_{10}O_{28}•4H_2O$ **C1**				$(NH_4)_2[Ni(H_2O)_6]_2V_{10}O_{28}•4H_2O$ **C2**			
Atoms	Angles °	Atoms	Angles °	Atoms	Angles °	Atoms	Angles °
O15–Co1–O16	88.10(8)	V1–O13^{i} –V2	85.91(5)	O16–Ni1–O17	176.13(9)	V5–O6–V4^{i}	88.11(6)
O15–Co1–O17	92.96(8)	V1–O13^{i} –V3	83.85(5)	O16–Ni1–O18	90.60(9)	V3–O6^{i}—V4	93.75(7)
O15–Co– O18	88.61(7)	V1–O13^{i} –V4	86.06(5)	O16–Ni1–O19	89.49(9)	V2–O8–V5	114.29(9)
O15–Co1–O19	87.47(8)	V1–O13^{i} –V5	86.34(6)	O16–Ni1–O20	87.15(9)	V2–O9–V3	99.44(8)
O15–Co1–O20	174.59(8)	V2–O13^{i}–V3	86.30(5)	O16–Ni1–O21	89.41(9)	V2–O9–V4	107.34(8)
O16–Co1–O17	90.93(9)	V2–O13^{i} –V4	170.00(8)	O17–Ni1–O18	91.42(9)	V3–O9–V4	106.98(8)
O16–Co1–O18	176.59(8)	V2–O13^{i} –V5	92.84(6)	O17–Ni1 O19	87.27(9)	V2–O10–V3	100.06(8)
O16–Co1–O19	92.77(8)	V3–O13^{i} –V4	86.91(6)	O17–Ni1 O20	96.29(9)	V2–O10–V4^{i}	107.14(8)
O16–Co1–O20	91.13(9)	V3–O13^{i} –V5	170.19(8)	O17–Ni1 O21	88.77(9)	V3–O10–V4^{i}	107.89(8)
O17–Co1–O18	88.32(7)	V4–O13^{i}–V5	92.59(6)	O18–Ni1–O19	88.27(9)	V3–O12–V5^{i}	114.74(9)
O17–Co1–O19	176.28(8)	V5–O14–V3^{i}	109.71(8)	O18–Ni1–O20	85.44(8)	V5–O15–V4^{i}	109.89(9)
O17–Co1–O20	92.41(8)	O1–V1–O2	102.90(8)	O18–Ni1–O21	176.55(9)	O1–V1–O5	102.32(9)
O18–Co1–O19	88.00(7)	O1–V1–O4	102.13(8)	O19–Ni1–O20	172.84(9)	O2–V1–O5	101.21(8)
O18–Co1–O20	92.22(8)	O1–V1–O5	102.44(8)	O19–Ni1–O21	95.17(9)	O3–V1–O5	102.65(9)
O19–Co1–O20	87.21(8)	O1–V1–O13^{i}	177.01(8)	O20–Ni1–O21	91.12(9)	O4–V1–O5	103.46(9)
V1–O2–V4	114.35(8)	O1–V1–O3	101.14(8)	V1–O1–V2	114.03(9)	O5–V1–O6	175.62(8)
V1–O3–V5	110.50(8)	O4–V2–O6	103.62(8)	V1–O2–V4	111.08(9)	O1–V2–O7	102.25(9)
V1–O4–V2	114.65(9)	O6–V2–O7	100.50(7)	V1–O3–V3^{i}	114.70(9)	O6–V2–O7	175.32(8)
V1–O5–V3	112.54(8)	O6–V2–O8	102.07(8)	V1–O4–V5	113.96(9)	O7–V2–O8	101.46(9)
V2–O7–V5	108.18(7)	O6–V2–O12^{i}	98.82(7)	V1–O6–V2	86.28(6)	O7–V2–O9	101.09(8)
V2–O7–V4^{i}	100.40(7)	O6–V2–O13^{i}	173.81(7)	V1–O6–V4	87.03(6)	O7–V2–O10	99.73(8)
V5–O7–V4^{i}	106.80(7)	O5–V3–O9	103.94(8)	V1–O6–V5	82.71(6)	O9–V3–O11	98.62(8)
V2–O8–V3	113.38(8)	O8–V3–O9	100.32(8)	V1–O6–V3^{i}	86.03(6)	O10–V3–O11	98.70(8)
V3–O10–V4	113.74(8)	O9–V3–O10	102.41(8)	V1–O6 V4^{i}	170.82(9)	O11–V3–O12	103.74(9)
V4–O12–V5	107.88(7)	O9–V3–O13^{i}	172.91(7)	V2–O6 V4^{i}	93.93(7)	O11–V3–O3^{i}	103.30(9)
V4–O12–V2^{i}	100.67(7)	O9–V3–O14^{i}	99.21(8)	V2–O6 V5	86.73(6)	O11–V3–O6^{i}	173.47(8)
V5–O12–V2^{i}	107.29(7)	O10–V4 –O11	102.21(8)	V2–O6–V3^{i}	169.80(9)	O4–V5–O14	103.53(9)
V5–O13–V1^{i}	172.48(8)	O11–V4–O12	100.38(8)	V2–O6–V4	92.78(7)	O6–V5–O14	173.96(8)
V5–O13–V2^{i}	93.93(6)	O11–V4–O7^{i}	98.41(8)	V4–O6–V5	169.66(9)	O8–V5–O14	101.50(9)
V5–O13–V3^{i}	88.63(6)	O11–V4–O13^{i}	174.14(7)	V4–O6–V3^{i}	92.35(6)	O14–V5–O15	99.85(8)
V5–O13–V4^{i}	93.25(6)	O2–V4–O11	103.50(8)	V4–O6–V4^{i}	102.15(7)	O14–V5–O12^{i}	102.72(9)
V5–O13–V5^{i}	101.18(7)	V5–O6–V3^{i}	85.66(6)				

Table 4 Selected hydrogen-bonding data (Å,°) and short contact distances (Å) in compounds **C1** and **C2**

$(NH_4)_2[Co(H_2O)_6]_2.V_{10}O_{28}{\bullet}4H_2O$ (C1)					$(NH_4)_2[Ni(H_2O)_6]_2.V_{10}O_{28}{\bullet}4H_2O$ (C2)				
D—H—A	d(D—H)	d(H—A)	d(D--A)	°(D—H--A)	D—H—A	d(D—H)	d(H—A)	d(D--A)	°(D—H--A)
N1—H4--O4	0.85(3)	2.010	2.838	162.38	N1—H1b--O11	0.95(5)	2.018	2.963	177.57
N1—H2--O8	0.83(4)	2.031	2.853	173.24	N1—H1c--O1s	0.90(4)	1.967	2.836	161.51
O17—H17a--O8	0.81(3)	1.988	2.797	174.83	O20—H20a--O1	0.71(3)	2.011	2.717	174.47
O15—H5b--O12	0.74(3)	1.920	2.659	176.20	O17—H17b--O8	0.75(4)	1.932	2.668	167.25
Ow1—H1wa--O10	0.88(2)	1.876	2.742	166.18	O18—H18a--O4	0.78(4)	1.987	2.747	166.50
					O1s—H1sb--O14	0.74(4)	2.148	2.884	172.52
					O2s—H2sa--O3	0.68(5)	2.264	2.913	159.88

Short Contact Distances (Å)					Short Contact Distances (Å)				
		Symm		Length	Length-VdW			Symm		Length	Length-VdW
Anion – Anion						**Anion – NH_4**					
O1	O1	−0.5 + x,1.5-y,-0.5 + z		2.992	−0.048	V5	H1D	x,-1 + y,1 + z		3.143	−0.057
Anion – NH_4						O7	N1	x,y,1 + z		2.843	−0.227
V1	H1	1-x,y,1.5-z		3.138	−0.062	O7	H1A	x,y,1 + z		2.660	−0.060
V1	H4	x,y,z		3.112	−0.088	O7	H1B	x,y,1 + z		2.547	−0.173
V2	H2	-1/2 + x,1/2 + y,z		3.039	−0.161	O12	N1	1 + y,1 + z		2.819	−0.251
O1	N1	1-x,y,1.5-z		2.964	−0.106	O12	H1D	1 + y,1 + z		2.044	−0.676
O1	H1	x,y,z		2.555	−0.165	**$Ni(H_2O)_6$—Anion**					
O3	H3	1-x,y,1.5-z		2.716	−0.004	O16	O9	x,1 + y,z		2.745	−0.295
$Co(H_2O)_6$ – Anion						O17	O7	−1 + x,1 + y,z		2.932	−0.108
O17	O2	0.5-x,0.5 + y,1.5-z	2.684		−0.356	O18	O3	x,y,z		2.999	−0.041
O16	O5	0.5-x,0.5 + y,1.5-z	2.962		−0.078	O19	O11	-1 + x,1 + y,z		3.024	−0.016
O19	O5	x,1-y,0.5 + z	2.681		−0.359	O21	O8	-1 + x,1 + y,z		2.848	−0.192
O19	O6	1-x,y,1.5-z	2.789		−0.251	O21	O2	x,1 + y,z		2.831	−0.209
O18	O7	1-x,y,1.5-z	2.705		−0.335	H17A	O7	-1 + x,1 + y,z		2.289	−0.431
O15	O9	x,1-y,0.5 + z	2.851		−0.189	H17B	V5	1-x,1-y,1-z		3.091	−0.109
$Co(H_2O)_6$—NH4						H19A	V3	-1 + x,1 + y,z		3.188	−0.012
Co1	H3	1-x,y,1.5-z	3.177		−0.023	H19A	O10	-1 + x,1 + y,z		2.683	−0.037
O15	N1	1-x,y,1.5-z	2.983		−0.087	H19A	O11	-1 + x,1 + y,z		2.361	−0.359
O15	H3	1-x,y,1.5-z	2.205		−0.515	H21A	O8	-1 + x,1 + y,z		2.178	−0.542
O19	N1	1-x,y,1.5-z	2.939		−0.131	H16A	O11	1-x,-y,2-z		2.689	−0.031
O19	H4	1-x,y,1.5-z	2.615		−0.105	H18B	O3	x,y,z		2.356	−0.364
						H17B	O8	1-x,1-y,1-z		1.932	−0.788
Anion—H_2Osolv						H18A	O4	1-x,1-y,1-z		1.987	−0.733
V3	H1WA	x,y,z		3.056	−0.144	H20A	V1	1-x,1-y,1-z		3.184	−0.016
O9	O1W	-x,y,1/2-z		2.992	−0.048	H20A	O1	1-x,1-y,1-z		2.011	−0.709
O9	H1WB	-x,y,1/2-z		2.694	−0.026	H16B	V3	x,1 + y,z		3.152	−0.048
O11	O1W	1/2 + x,1/2 + y,z		2.907	−0.133	H16B	O9	x,1 + y,z		2.035	−0.685
O11	H1WB	1/2 + x,1/2 + y,z		2.460	−0.260	H2OB	V2	x,1 + y,z		3.036	−0.164
O6	O1S	x,y,z		2.848	−0.192	H2OB	O1	x,1 + y,z		1.956	−0.764
O6	H1SB	x,y,z		1.999	−0.721	H21B	V4	x,1 + y,z		3.108	−0.092
O9	O1S	1/2-x,1/2 + y,1.5-z		2.870	−0.170	H21B	O2	x,1 + y,z		2.025	−0.695
O1W	O1W	-x,y,1/2-z		2.781	−0.259	**Anion—H_2Osolv**					
O1S	O1S	-x,y,1.5-z		2.847	−0.193	O5	H1SA	x,-1 + y,1 + z		2.348	−0.372
O1S	H1SA	-x,y,1.5-z		2.578	−0.142	O14	H1SA	-1 + x,-1 + y,1 + z		2.607	−0.113
						$Ni(H_2O)_6$—H_2Osolv					
						O19	O1S	1-x,1-y,1-z	2.937		−0.103
						H19B	O1S	1-x,1-y,1-z	2.149		−0.571

Table 4 (continued)

Short Contact Distances (Å)				Short Contact Distances (Å)					
		Symm	Length	Length-VdW			Symm	Length	Length-VdW
					O16	O2S	x,y,1 + z	2.836	−0.204
					H16A	O2S	x,y,1 + z	2.133	−0.587
					H16A	H2SB	x,y,1 + z	2.317	−0.083

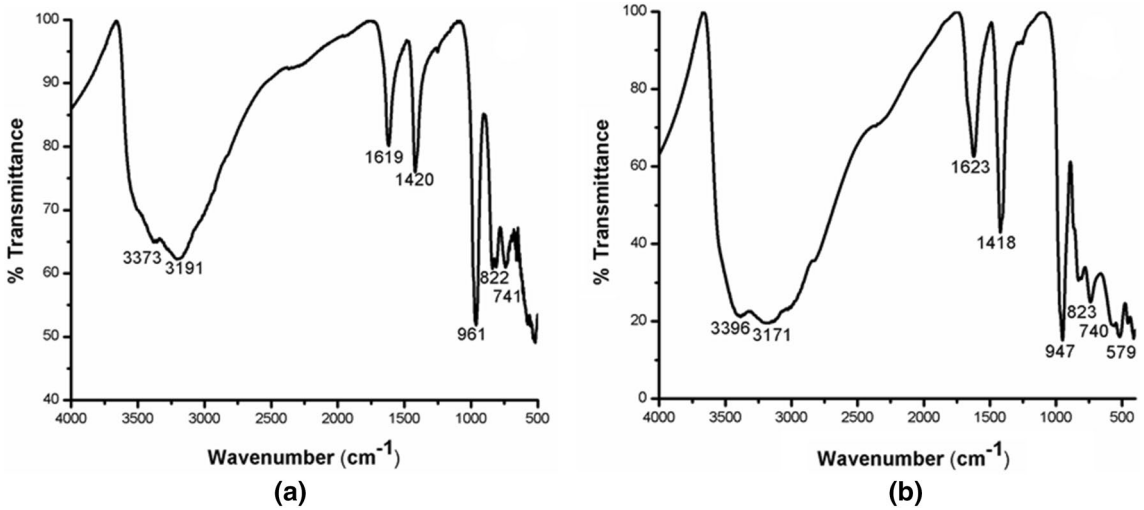

Fig. 3 FT-IR spectra of **a** $(NH_4)_2[Co(H_2O)_6]_2.V_{10}O_{28}{\cdot}4H_2O$ **C1** and **b** $(NH_4)_2[Ni(H_2O)_6]_2.V_{10}O_{28}{\cdot}4H_2O$ **C2**

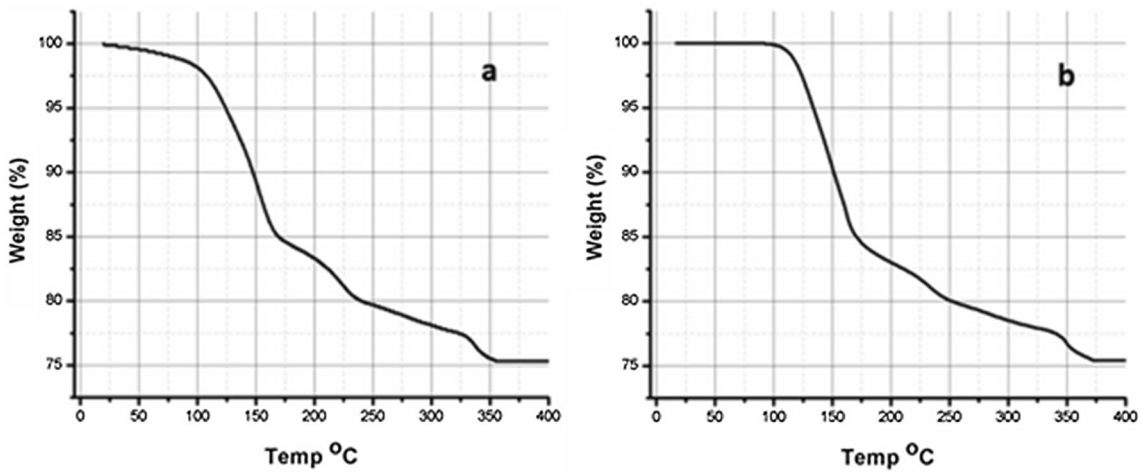

Fig. 4 TGA curves of **a** $(NH_4)_2[Co(H_2O)_6]_2.V_{10}O_{28}{\cdot}4H_2O$ and b $(NH_4)_2[Ni(H_2O)_6]_2.V_{10}O_{28}{\cdot}4H_2O$

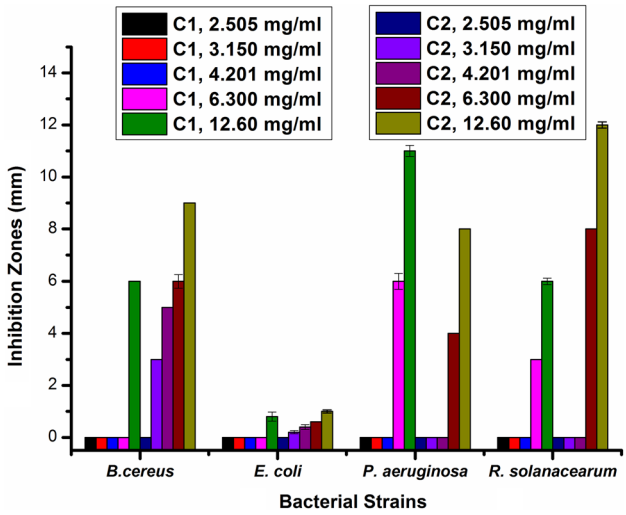

Fig. 5 Antibacterial activities of **C1** and **C2**, indicated by the inhibition zone diameter (mm), against the four tested bacterial strains

Table 5 Minimum inhibitory concentrations (MICs) of **C1** and **C2** in mg/ml against the four tested bacterial strains

	$(NH_4)_2[Co(H_2O)_6]_2V_{10}O_{28}{\cdot}4H_2O$ (**C1**, mg/ml)	$(NH_4)_2[Ni(H_2O)_6]_2V_{10}O_{28}{\cdot}4H_2O$ (**C2**, mg/ml)
B. cereus ATCC 33,018	12.60	3.150
E. coli O157	12.60	3.150
P. aeruginosa ATCC 9027	6.300	6.300
R. solanacearum	6.300	6.300

Funding Open access funding provided by The Science, Technology & Innovation Funding Authority (STDF) in cooperation with The Egyptian Knowledge Bank (EKB).

Declarations

Conflict of interest This research did not receive any specific grant from funding agencies in the public, commercial, or not-for-profit sectors.

References

1. D.-L. Long, R. Tsunashima, and L. Cronin (2010). *Angew. Chem. Int. Ed.* **49**, 1736.
2. M. Sadakane and E. Steckhan (1998). *Chem. Rev.* **98**, 219.
3. S.-S. Wang and G.-Y. Yang (2015). *Chem. Rev.* **115**, 4893.
4. H. Lv, Y. V. Geletii, C. Zhao, J. W. Vickers, G. Zhu, Z. Luo, J. Song, T. Lian, D. G. Musaev, and C. L. Hill (2012). *Chem. Soc. Rev.* **41**, 7572.
5. J. M. Clemente-Juan, E. Coronado, and A. Gaita-Ariño (2012). *Chem. Soc. Rev.* **41**, 7464.
6. T. Ruther, V. M. Hultgren, B. P. Timko, A. M. Bond, W. R. Jackson, and A. G. Wedd (2003). *J. Am. Chem. Soc.* **125**, 10133.
7. J. T. Rhule, C. L. Hill, D. A. Judd, and R. F. Schinazi (1998). *Chem. Rev.* **98**, 327.
8. A. Bijelic, M. Aureliano, and A. Rompel (2018). *Chem. Commun.* **54** (10), 1153.
9. N. Fukuda and T. Yamase (1997). *Biol. Pharm. Bull.* **20**, 927.
10. S. Aschwanden, H. W. Schmalle, A. Reller, and H. R. Oswald (1993). *Mater. Res. Bull.* **28**, 575.
11. E. E. Hamilton, P. E. Fanwick, and J. J. Wilker (2002). *J. Am. Chem. Soc.* **124**, 78.
12. J. Li, C. Wei, D. GuO, C. Wang, Y. Han, G. He, J. Zhang, X. Huang, and C. Hu (2020). *Dalton Trans.* **49**, 14148.
13. V. W. Day, W. G. Klemperer, and O. M. Yaghi (1989). *J. Am. Chem. Soc.* **111**, 4518.
14. E. Sánchez-Lara, A. Pérez-Benítez, S. Treviño, A. Mendoza, F. Meléndez, E. Sánchez-Mora, S. Bernès, and E. González-Vergara (2016). *Crystals* **6**, 65.
15. T. Kurata, Y. Hayashi, and K. Isobe (2010). *Chem. Lett.* **39**, 708.
16. D. Hou, K. D. Hagen, and C. L. Hill (1992). *J. Am. Chem. Soc.* **114**, 5864.
17. D. Hou, K. S. Hagen, and C. L. Hill (1993). *J. Chem. Soc. Chem. Commun.* **4**, 426.
18. J. Marrot, K. Barthelet, C. Simonnet, and D. Riou (2005). *C.R. Chim.* **8**, 971.
19. M. Aureliano (2009). *Dalton Trans.* **42**, 9093.
20. A. Gorzsás, I. Andersson, and L. Pettersson (2006). *Eur. J. Inorg. Chem.* **18**, 3559.
21. A. Xie, C.-A. Ma, L. Wang, and Y. Chu (2007). *Electrochim. Acta* **52**, 2945.
22. T. L. Turner, V. H. Nguyen, C. C. McLauchlan, Z. Dymon, B. M. Dorsey, J. D. Hooker, and M. A. Jones (2012). *J. Inorg. Biochem.* **108**, 96.
23. S. Hua, G. Inesi, and C. Toyoshima (2000). *J. Biol. Chem.* **275**, 30546.
24. T. Tiago, M. Aureliano, and C. Gutierrez-Merino (2004). *Biochemistry* **43**, 5551.
25. E. G. Demaster and R. A. Mitchell (1973). *Biochemistry* **12**, 3616.
26. G. Soman, Y. C. Chang, and D. J. Graves (1983). *Biochemistry* **22**, 4994.
27. M. Zhao, X. Chen, G. Chi, D. Shuai, L. Wang, B. Chen, and J. Li (2020). *Inorg. Chem. Front.* **7**, 4320.
28. B. Mukherjee, B. Patra, S. Mahapatra, P. Banerjee, A. Tewari, and M. Chatterjee (2004). *Toxicol. Lett.* **150**, 135.
29. D. G. Barceloux (1999). *J. Toxicol. Clin. Toxicol.* **37**, 265.
30. F. Zhai, X. Wang, D. Li, H. Zhang, R. Li, and L. Song (2009). *Biomed. Pharmacother.* **63**, 51.
31. V. Dimitrova, K. Zhetcheva, and L. P. Pavlova (2011). *J. Chem.* **35**, 215.
32. G.A.-E. Mahmoud, A. B. M. Ibrahim, and P. Mayer (2021). *ChemistrySelect* **6** (15), 3782.
33. D. Rehder (2013). *Dalton Trans.* **42**, 11749.
34. S. Hatamie, M. Nouri, S. K. Karandikar, A. Kulkarni, S. D. Dhole, and D. M. Phase (2012). *Mater Sci. Eng. C* **32**, 92.

35. E. L. Chang, C. Simmers, and D. A. Knight (2010). *Pharmaceuticals* **3**, 1711.
36. L. Yang, D. C. Crans, S. M. Miller, A. la Cour, O. P. Anderson, P. M. Kaszynski, M. E. Godzala, L. D. Austin, and G. R. Willsky (2002). *Inorg. Chem.* **41**, 4859.
37. F. Dimiza, A. N. Papadopoulos, V. Tangoulis, V. Psycharis, C. P. Raptopoulou, D. P. Kessissoglou, and G. Psomas (2010). *Dalton Trans.* **39**, 4517.
38. R. Bartha and E. J. Ordal (1965). *J. Bacteriol.* **89**, 1015.
39. R. P. Hausinger (1987). *Microbiol. Rev.* **51**, 22.
40. G. Fierros-Romero, J. A. Wrosek-Cabrera, M. Gomez-Ramırez, R. C. Pless, A. M. Rivas-Castillo, and N. G. Rojas-Avelizapa (2017). *Curr. Microbiol.* **74**, 840.
41. D. U. Miodragovic, G. A. Bogdanovic, Z. M. Miodragovic, M. D. Radulovic, S. B. Novakovic, G. N. Kaluderovic, and H. Kozlowski (2006). *J. Inorg. Biochem.* **100**, 1568.
42. K. Nomiya, A. Yoshizawa, K. Tsukagoshi, N. C. Kasuga, S. Hirakawa, and J. Watanabe (2004). *J. Inorg. Biochem.* **98**, 46.
43. M. C. Rodriguez-Argüelles, S. Mosquera-Vazquez, J. Sanmartin-Matalobos, A. M. Garcia-Deibe, C. Pelizzi, and F. Zani (2010). *Polyhedron* **29**, 864.
44. K. Matsumoto, S. Yamamoto, Y. Yoshikawa, M. Doe, Y. Kojima, H. Sakurai, H. Hashimoto, and M. N. Kajiwara (2005). *Bull. Chem. Soc. Jpn.* **78**, 1077.
45. P. Dorkov, I. N. Pantcheva, W. S. Sheldrick, H. Mayer-Figge, R. Petrova, and M. Mitewa (2008). *J. Inorg. Biochem.* **102**, 26.
46. J. Lv, T. Liu, S. Cai, X. Wang, L. Liu, and Y. Wang (2006). *J. Inorg. Biochem.* **100**, 1888.
47. E. Podda, M. Arca, G. Atzeni, S. J. Coles, A. Ibba, F. Isaia, V. Lippolis, G. Orrù, J. B. Orton, A. Pintus, E. Tuveri, and M. C. Aragoni (2020). *Molecules* **25**, 2052.
48. A. Simo, M. Drah, N. R. S. Sibuyi, M. Nkosi, M. Meyer, and M. Maaza (2018). *Ceram. Int.* **44** (7), 7716.
49. I. Kamika and M. N. B. Momba (2013). *Desalination Water Treat.* **51**, 7431.
50. Bruker, SMART and SAINT (2008) Bruker AXS Inc., Madison, WI
51. G. M. Sheldrick, *SADABS* (Bruker AXS Inc., Madison, WI, 2004).
52. G. M. Sheldrick (2015). *Acta Crystallogr.* **71**, 3.
53. L. J. Farrugia (1999). *J. Appl. Crystallogr.* **32**, 837.
54. C. F. Macrae, I. J. Bruno, J. A. Chisholm, P. R. Edgington, P. McCabe, E. Pidcock, L. Rodriguez-Monge, R. J. Taylor, J. Van De Streek, and P. A. Wood (2008). *J. Appl. Crystallogr.* **41**, 466.
55. I. Wiegand, K. Hilpert, and R. E. W. Hancock (2008). *Nat. Protoc.* **3** (2), 163.
56. L. Klistincova, E. Rakovsky, and P. Schwendt (2010). *Transit. Met. Chem.* **35**, 229.
57. S. Du, N. Zho, and X. Wu (1994). *Polyhedron* **13**, 301.
58. C. Li, D. Zhong, X. Huang, G. Shen, Q. Li, J. Du, Q. Li, S. Wang, J. Li, and J. Dou (2019). *New J. Chem.* **43**, 5813.
59. S. Li, Z. Li, J. Zhang, Z. Su, S. Qi, S. Guo, and X. Tan (2017). *J. Chem. Sci.* **129** (5), 573.
60. L. Krivosudsky, A. Roller, and A. Rompel (2019). *New J. Chem.* **43**, 17863.
61. E. Sánchez-Lara, I. Sánchez-Lombardo, A. Pérez-Benítez, Á. Mendoza, M. Flores-Álamo, and E. G. Vergara (2015). *J. Clust. Sci.* **26**, 901.
62. Z. J. Zhong, X. Z. You, and Q. C. Yang (1994). *Polyhedron* **13**, 1951.
63. X. Li, L. Yan, H. Wanyan, and R. Yang (1993). *Polyhedron* **13**, 2021.
64. I. Mestiri, B. Ayed, and A. Haddad (2013). *J. Clust. Sci.* **24**, 85.
65. E. Feacium, S. Toumi, N. Ratel-Ramond, and S. Akriche (2015). *J. Clust. Sci.* **26**, 1821.